Tribology Letters (2022) 70:115
https://doi.org/10.1007/s11249-022-01657-5

TRIBOLOGY METHODS

Frictionless vs. Frictional Contact in Numerical Wear Predictions of Conformal and Non-conformal Sliding Couplings

Lorenza Mattei[1] · **Francesca Di Puccio**[1]

Received: 29 July 2022 / Accepted: 13 September 2022

Abstract
The role of friction on wear evolution is manifold since it interplays with lubrication regime, nominal contact point, and contact pressure distribution. Nevertheless, in the literature many wear models simulate wear assuming frictionless contact conditions to simplify the analyses. That assumption, physically not realistic, often appears as a contradiction, permitted in numerical simulations where friction and wear can be considered independent phenomena.
This study aims to validate the frictionless assumption in wear models with steady nominal contact point, such as in many common configurations, e.g. pin on plate/pin on disc. Wear was simulated according to the Archard wear law for both non-conformal and conformal pin-on-plate contact pairs in reciprocating motion, assuming frictionless and frictional contact conditions, varying the coefficient of friction f in the range 0–0.4. Finite Element wear models were developed in Ansys® both with implicit and explicit kinematics. Results demonstrate that the effect of friction on contact pressure distribution and worn profiles and on their evolution is negligible (differences lower than 0.05%). Thus, wear can be predicted using models in frictionless conditions which allow to extremely reduce the computational costs that represent a limit of FE wear simulations. Additionally, a procedure with implicit kinematics was compared to the explicit one resulting valid and computationally convenient, especially in case of non-conformal contact.

Keywords FE wear modelling · Kinetic friction · Reciprocating sliding contact · Pin on plate · Conformal coupling · Non-conformal coupling

1 Introduction

Numerical wear simulations are a powerful tool to predict the evolution of contact parameters during the service life of engineering components, from mechanical ones, like gears [1–3] or wheel-rail pair [4] to biomedical devices, like joint implants [5, 6]. Different approaches can be adopted to develop wear models: rarely pure analytical methods [5, 7, 8], whilst more commonly Finite Element (FE) analyses [2, 6, 9–12]. Each method has pros and cons: analytical models allow fast simulations typically for the running-in phase of the wear process [7, 8], whilst FE models can be used for long-term wear predictions to the detriment of high computational costs [13, 14]. Independently from the used method, wear models are typically based on the implementation of a wear law that relates the wear volume to contact conditions, i.e. contact force/pressure and sliding velocity between the coupling surfaces. Most of the wear models in the literature are based on the Archard wear law that holds for abrasive and adhesive wear of hard surfaces. In global form, for surfaces in relative translation, it states

$$V = k F_{\mathrm{N}} s \tag{1}$$

where V is wear volume, k is wear coefficient, F_{N} the load normal to the contact and s, the sliding distance. The wear law is often used in its local form, valid at any point P of the contact surface, at a given instant t

$$\dot{h}\,(P,t) = k\,p\,(P,t)\,v\,(P,t) \tag{2}$$

where $\dot{h}$ is the wear rate, p the contact pressure and v the magnitude of the sliding velocity.

In wear models based on the Archard law, the contact is modelled as dry, neglecting the presence of wear debris: the

✉ Lorenza Mattei
lorenza.mattei@unipi.it

[1] Department of Civil and Industrial Engineering, Largo Lucio Lazzarino 2, 56126 Pisa, Italy

Published online: 28 September 2022

effect of the lubricant, and thus the lubrication regime, are included in the value of k experimentally estimated.

Consequently, the critical aspect of the wear laws is the accurate estimation of the wear coefficient [7, 15] which depends on many factors amongst which friction, lubrication regime, material properties of the mating surfaces, kinematic, and loading conditions. Additionally, k can even change in time and locally, such as in case of cross-shear [6, 16].The wear law and wear model validation is a further critical issue [7, 17].

The focus of this study is on the effect of friction on wear simulations, with the aim of clarifying an apparent contradiction: whilst wear is surely caused by a frictional contact, models are often based on the frictionless contact hypothesis [18, 19]. Despite being not physically reasonable, this assumption is frequently used in wear simulations, where friction and wear can be considered independent, to simplify the analyses. To clarify the latter point it should be considered that friction can affect contact and wear in multiple ways. Firstly, friction interplays with the lubrication regime and thus affects the wear coefficient, being so included in Eqs. (1–2) through k itself. Secondly, it can cause a displacement of the nominal contact point and consequently the magnitude of normal component of the contact force and of the contact pressure. That applies for instance to ball in socket joints, such as hip joint implants, as treated in [8], but not for more common and simpler conditions, like pin-on-plate and pin-on-disc wear tests. Finally, friction can also affect the contact pressure distribution and thus the wear rate of Eq. (2) through p.

Consequently, for cases where the friction does not cause a change neither of the nominal contact point nor of the contact pressure distribution, e.g. pin-on-plate tests, the contact can be simulated as frictionless, as friction is implicitly included in the wear model through k. That allows, on the one hand, to extremely reduce the high computational costs of FE wear models and, on the other hand, to widen the field of application of the analytical wear models to frictional cases. Indeed, the latter is based on contact pressure solutions valid for frictionless contact, e.g. according to the Hertzian theory, for non-conformal hard-on-hard coupling, and the Bartel's theory [20], for conformal soft on-hard couplings.

Although a few literature studies declare that the effect of friction on the contact pressure distribution is negligible, e.g. [9, 10, 21, 22], to the best of authors' knowledge none has deepened the matter.

The objective of this study is to investigate the effect of friction on contact pressure and wear evolution in both non-conformal and conformal contacts. FE models of the sliding contact of pin-on-plate tests were developed in Ansys® and a sensitivity analysis of pressure and wear depth profiles to the friction coefficient was carried out for values of f in the range 0–0.4.

2 Materials and Methods

2.1 Case Study: Pin-on-Plate Wear Tests

A pin-on-plate wear test was selected as case study, with pin and plate in reciprocating sliding motion. Two cases were simulated, as shown in Fig. 1a, differing only for the pin geometry:

1) Non-conformal contact between a half-cylindrical pin and a rectangular plate (on the left) (non-conformal model, NCM).
2) Conformal contact between a flat-ended pin and a rectangular plate (on the right) (conformal model, CM).

FE models of these case studies were developed in ANSYS Workbench®, exploiting APDL commands for wear implementation (see Sect. 2.6).

2.2 Geometry and Materials

According to the literature [9, 10, 18], the problem can be modelled as a plane strain case, and the geometry simplified with its 2D section (Fig. 1b).

The non-conformal contact pair is characterized by a half-cylindrical pin of radius $R = 10$ mm and a rectangular plate of dimensions $6R$xR. The conformal pair differs from the NCM for the geometry of the pin that has a flat end of dimensions $2R$xR and with a fillet radius $r = 2.5$ mm.

For both models, pin was considered made of steel with a 200 GPa Young modulus and a Poisson ratio of 0.3. The plate was assumed rigid for two reasons: a case of monolateral wear affecting only pin was considered; the rigid assumptions allow to drastically reduce the computational time. However, the results remain valid for the case of flexible-on-flexible contact.

2.3 Mesh

In both models, the pin was meshed with linear quadrilateral element, PLANE 182. The mesh size was not uniform in the pin, varying from 1 mm far from the contact region down to 20 µm close to it (Fig. 1c). A sub-region (1 mm × 4 mm) was created close to the contact with rectangular elements of size 20 µm × 25 µm to avoid mesh distortion (squat elements) caused by worn material removal. The contact surfaces were meshed with CONTA172 and TARGE169 elements (see contact details in Sect. 2.4). The mesh size was selected through a sensitivity analysis on the contact pressure at the

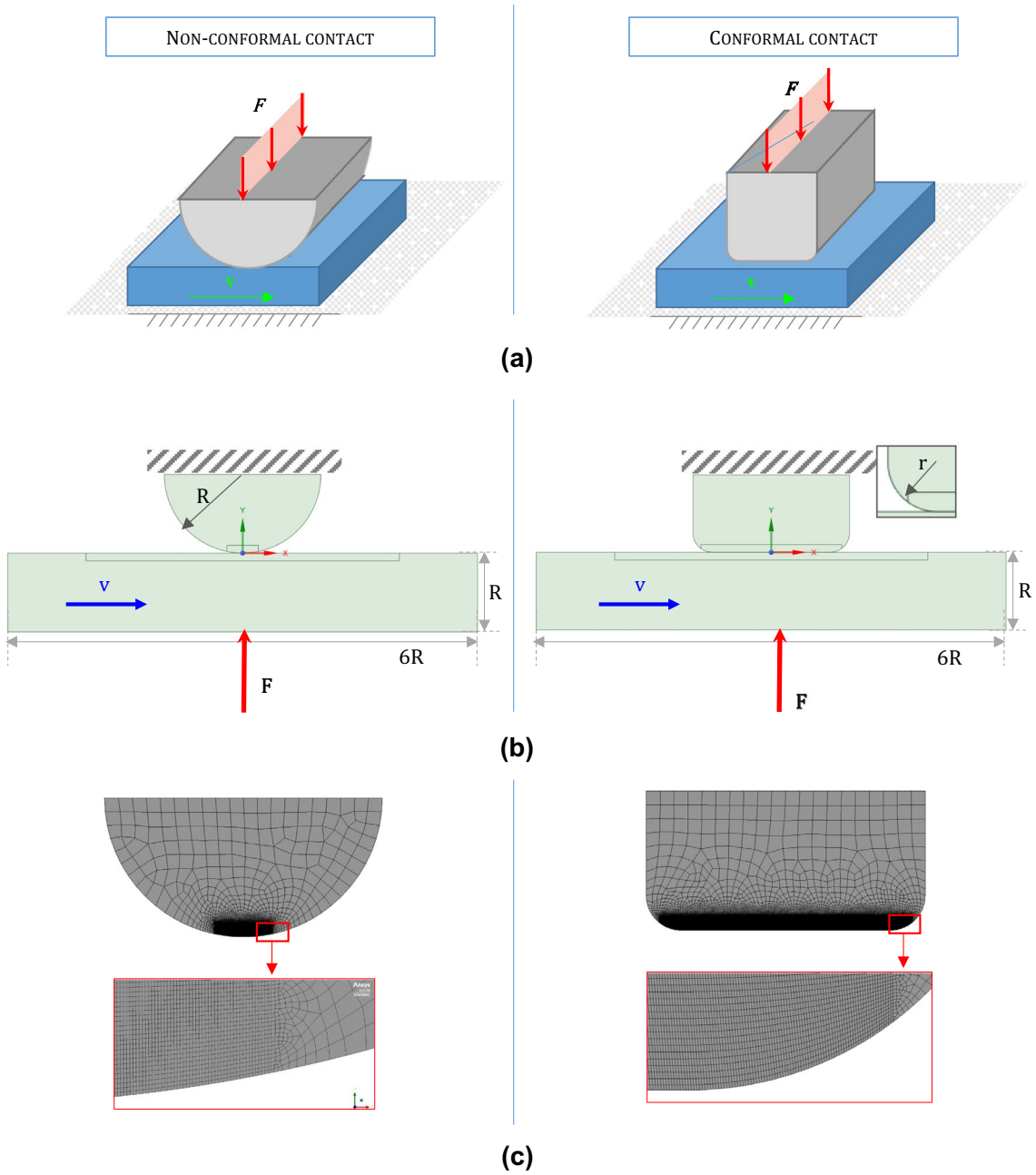

Fig. 1 Case studies: pin-on-plate wear tests for non-conformal (left column) and conformal contact (right column). **a** General scheme. **b** Model geometry and loading and kinematics conditions. **c** Mesh of the pins with detail of the refined sub-regions close to the contact

centre of the contact area. In case of NCM, the described mesh produces an error of 2.5% on the maximum contact pressure with respect to the Hertzian solution.

2.4 Surface Interactions

Both for NCM and CM, several types of contact were simulated from frictionless to frictional, with a friction coefficient value in the range 0.05–0.4. The contact was simulated as asymmetric (*behaviour* setting), with the pin chosen as contact region and the plate as target one. Other specific contact settings were Augmented Lagrange as formulation and Nodal-normal to target as detection method.

2.5 Kinematic and Loading Conditions

The reciprocating sliding motion of a pin-on-plate set-up under constant load was simulated according to the boundary conditions shown in Fig. 1b. Both in NCM and CM, the top edge of pin was built-in whilst motion and load were applied to the bottom edge of the plate through remote force and remote displacement, respectively. A wear cycle was given by the sequence of an outbound and a return stroke, with the stroke length $s = 2R$, under a constant load of 100 N. In the outbound stroke, the pin translated from $x = -R$ to $x = \mathrm{R}$, whilst in the return stroke it translated back to initial position. The stroke was covered in 1 s, thus resulting in a relative velocity between pin and plate $v = 10$ mm/s. The number of simulated strokes was set to $N = 20$ for the standard simulations and $N = 1000$ for the "accelerated" ones (see Sect. 2.6) corresponding to a travel distance of 400 mm and 20 m, respectively.

2.6 Wear Law and Wear Implementation

The pin wear was predicted according to the Archard wear law (Eq. (1–2)). The value of k was kept constant through simulations with different friction values, since the objective of the present study was to investigate the effect of friction on the contact pressure distribution and wear.

Wear was simulated through the introduction of an ADPL command in the contact environment. Ansys® includes a specific tool for automatic wear simulation through the command *TB WEAR* with option ARCD, which implements the generalized form of the Archard wear law, according to

$$\dot{h} = \frac{k}{H} p^m v^n, \tag{3}$$

where H is the material hardness, k is the wear coefficient, and m and n exponents of pressure and sliding velocity, respectively. The parameters of Eq. (3) are set through the *TBDATA* command, whilst the selection of time instants during which activate or deactivate wear is done using the *TBFIELD* command. When $H = m = n = 1$, Eq. (3) gives Eq. (2).

Both in NCM and CM, we assumed $k = 10^{-8}$ mm^2/N, $H = m = 1$, whilst the exponent n of the velocity was used to select between two different simulation procedures:

1) $n = 0$, Implicit Kinematics (IK): since the sliding velocity is constant in time and space (i.e. does not vary over the contact area), in case of frictionless contact, it is included directly in the k, assuming a new $k_{IK} = kv$ whilst the plate translation is not simulated (zero x displacement).
2) $n = 1$, Explicit Kinematics (EK): kinematics conditions are reproduced explicitly, through the plate translation. This procedure is necessary to simulate frictional cases, when the frictional actions developed at the contact surfaces are opposite to the sliding relative motion.

When the KE approach was used, the stroke was sampled in five points. The sampling frequency is fundamental for complex 3D and time-varying boundary conditions, but not in the present case since both the contact pressure distribution and the sliding velocity are constant throughout each wear cycle and the counterpart is rigid.

For the same reason, for the selected pin-on-plate case study, it can be convenient to introduce an acceleration factor N_a [18] so that an "accelerated" wear can be computed according to Eq. (3), including the N_a in the wear coefficient and thus $k_{IKa} = N_a kv$ and $k_{EKa} = N_a k$, respectively, in IK and EK procedures. The accelerated wear was simulated only for the CM, for $N_a = 50$, to achieve wear depths of the same magnitude order of the NCM ones.

2.7 Simulations Plan

Table 1 summarizes the simulations performed for NCM and CM, both with an implicit and explicit kinematics description, by varying the friction coefficient in the range 0–0.4. Simulations ran on a pc equipped with a processor Intel(R) Xeon(R) Silver 4214R CPU@2.40 GHz and 64 GB Ram.

3 Results and Discussion

The main results consist in the comparison of the evolution of contact pressure and worn geometry profiles during wear damaging, for the frictionless and the frictional cases (top

Table 1 Simulations plan

Model	IK/EK	N_a	f
NCM	IK	1	0
	EK	1	0, 0.05, 0.1, 0.15, 0.2, 0.3, 0.4
CM	IK	1	0
	EK	1	0, 0.05, 0.1, 0.15, 0.2, 0.3, 0.4
	IK	10	0
	EK	10	0, 0.4

NCM non-conformal contact model, *CM* conformal contact model, *IK* implicit kinematics, *EK* implicit kinematics acceleration factor *N*a, friction coefficient *f*

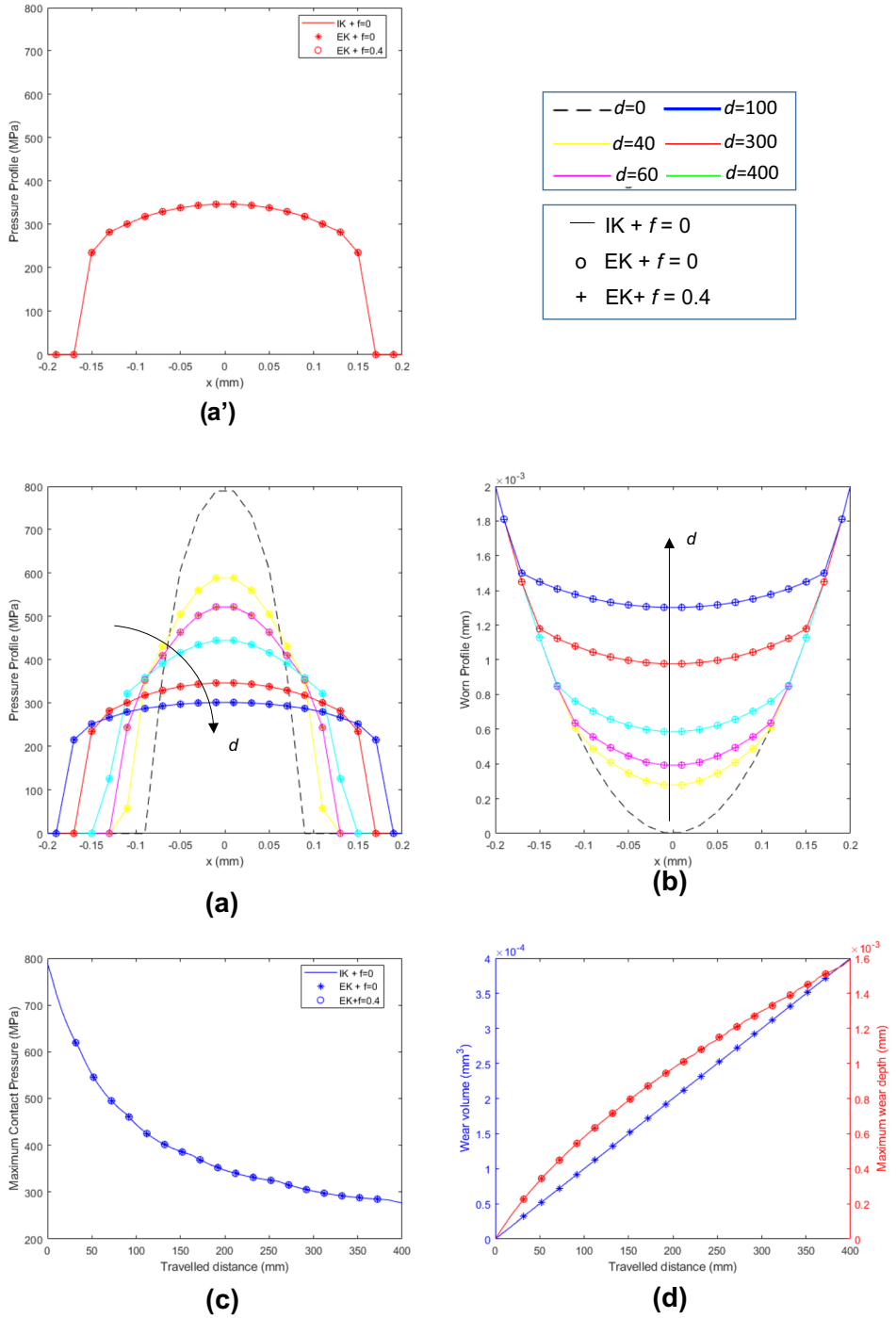

Fig. 2 NCM results for frictionless and frictional contacts: evolution of the contact pressure profile **a** and of the worn profile **b**; variation of the maximum contact pressure **c**, maximum wear depth, and wear volume **d** with the travelled distance. Image **a'** helps in understanding the legend: colours are used to distinguish data obtained for different travelled distances, continuous line for IK results, and symbols for EK results (Color figure online)

of Figs. 2 and 4). The time histories of pressure and wear depth at the centre of the worn regions were also considered (bottom of Figs. 2 and 4)). Additionally, two different approaches for the frictionless cases, based on the implicit and explicit kinematics simulations, were compared.

3.1 Non-conformal Contact Model

3.1.1 Wear Evolution

Figure 2 summarizes the main results obtained from the NCM. According to the literature [9, 10, 18], the evolution

of the contact pressure (Fig. 2a) and worn profiles (Fig. 2 b) demonstrated that wear causes a more and more conformal contact, independently from the friction coefficient. The pin profile tends to flatten along with the contact pressure one: the pin curvature radius increases, whilst the contact pressure decreases being distributed over a wider contact area.

As shown in Fig. 2c, the maximum contact pressure, located at the centre of the contact area (at the pin axis), decreases rapidly with the travelled distance during the running-in and then more slowly, when approaching to the steady state, passing from the initial value of 815 MPa to final one of 277 MPa. That is in agreement with the non-linear trend of the maximum wear depth (same location, at the pin axis) whose rate decreases passing from the running-in to the steady-state phase (Fig. 2c). A maximum wear depth of 1.6 μm was predicted for the total sliding distance of 400 mm. It is worth remarking how a very thin layer of worn material causes a significant change in the contact conformity and contact pressure. Thus, the steady-state phase is characterized by an almost flat contact pressure and geometric profiles.

The simulated wear volume coincides with the one predicted by the Archard Wear law, i.e. a value of 4 10^{-4} mm^3 at the end of the simulated test.

3.1.2 Effect of Friction on Wear Evolution

Results pointed out that the effect of friction on wear predictions is absolutely negligible, with percentage differences on pressure/wear depth values lower than 0.05% between the frictionless and the frictional contact conditions. As an example, Fig. 2 compares results obtained for the two extreme cases: $f=0$ (obtained with both IK and EK approaches) and $f=0.4$: the correspondent curves are almost overlapped. Results from all the other models assuming a different value of f (see Table 1) are not reported being almost identical. Although the presence of friction does not modify the pressure distributions, it extremely affects computational costs. Histogram of Fig. 3 compares the computational times of the simulations by varying f value and demonstrates that it increases with f values up to threefold for $f=0.4$ compared to $f=0$. Consequently, the simulation of a frictional contact in wear predictions, on the one hand, is unnecessary to improve results accuracy and, on the other hand, it significantly increases the computational efficiency.

3.1.3 IK vs EK Procedures

As far as the frictionless case is concerned, IK and EK procedures were implemented. Results compared in Fig. 2 appear to be almost identical for the two cases. On the other hand, the computational cost of the EK simulation with $f=0$ was 30% higher that the IK one (Fig. 3) demonstrating that the IK is not only accurate as much as the EK, but also computationally more convenient.

3.2 Conformal Contact Model

3.2.1 Wear Evolution

Results obtained for the CM are summarized in Fig. 4. The pressure profile in unworn conditions is flat over almost all the contact area, with the exception near the fillets, characterized by peaks caused by the local change of curvature radius (Fig. 4a). For all the simulated cases, the pressure profile is not significantly affected by the wear: the main

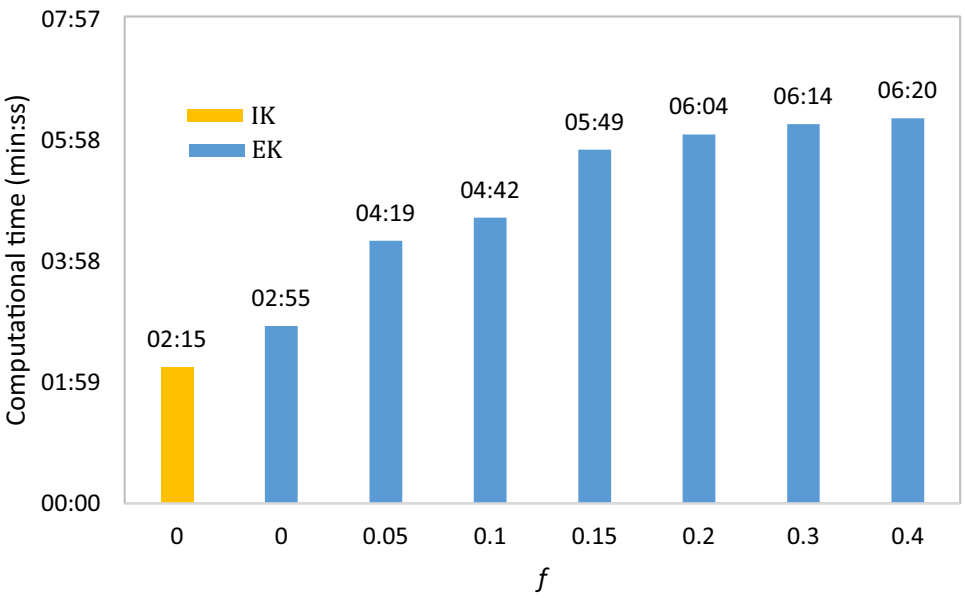

Fig. 3 Computational costs of NCM simulations in function of the f value

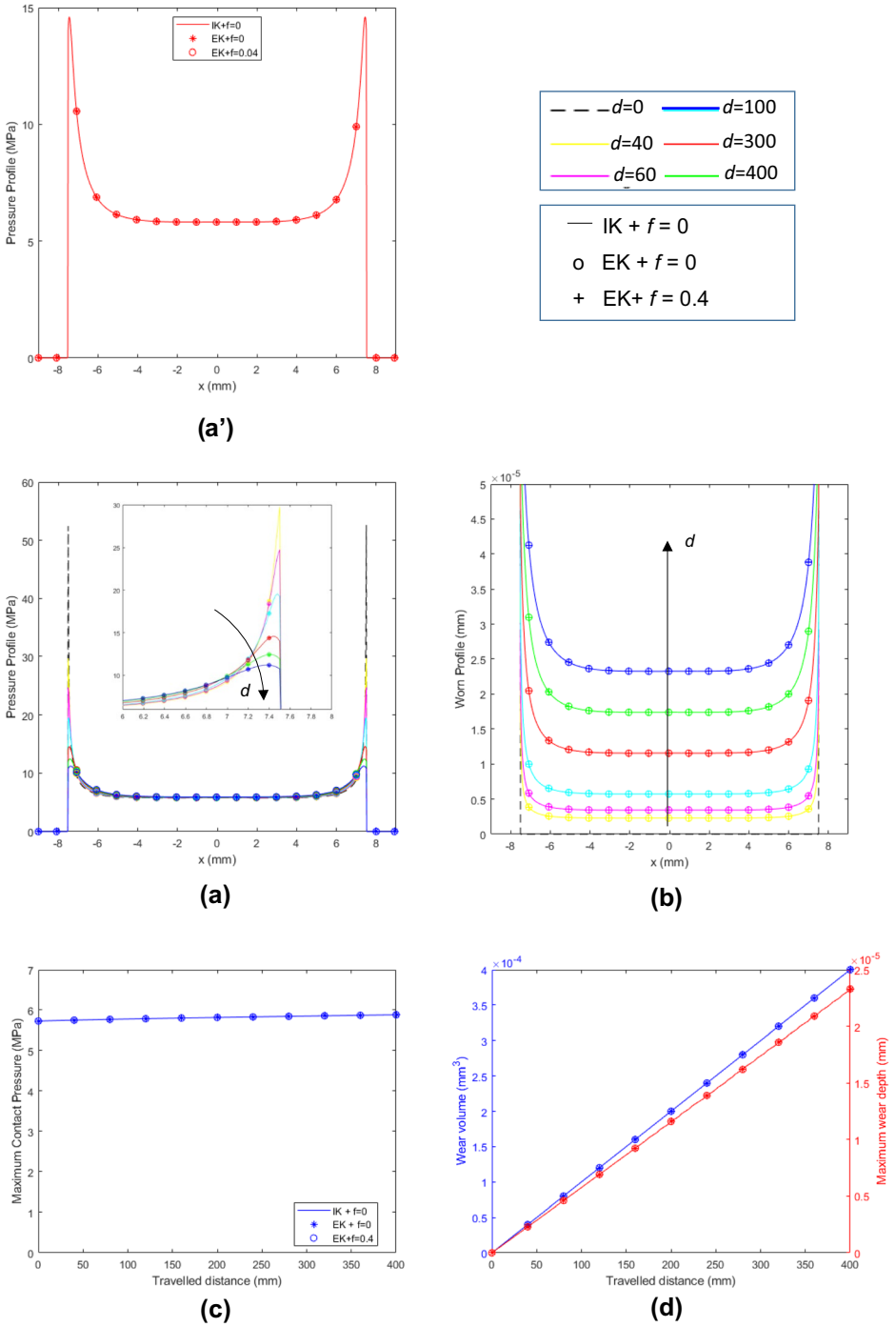

Fig. 4 CM results for frictionless and frictional contact: evolution of the contact pressure profile **a** and of the worn profile **b**; variation of the contact pressure **c** and maximum wear depth at the centre of the worn area, and wear volume **d** with the travelled distance. Image **a'** helps in understanding the legend: colours are used to distinguish data obtained for different travelled distances, continuous line for IK results, and symbols for EK results (Color figure online)

change consists in the decrease of the lateral peaks caused by a higher conformity of the edge of the contact region, close to the fillet, that is well captured by Fig. 4b which describes the evolution of the pin geometry which remains characterized by a flat profile. Accordingly, as wear progresses, the pressure at the centre of the contact area, at pin axis, remains almost constant, with only a slight increase from 5.7 MPa to 5.9 MPa due to a significant decrease of the lateral peaks (consider that, being the load constant, the pressure profiles must have the same integral over the contact area) (Fig. 4c). That is clearer in case of higher travelled distances (see Sec. 3.2.3). Differently from the NCM, the wear depth at the pin centre increases linearly with the travelled distance (Fig. 4d). Indeed, the node at the pin centre, as also the close nodes, undergoes to an almost constant contact pressure, in addition to a constant sliding velocity. Since the contact is conformal,

both the contact pressure and the wear depth at the pin axis resulted much lower than for the NCM, with a maximum wear depth of about 0.023 μm vs 1.6 μm of NCM) at pin axis.

According to the Archard wear law, the final wear volume is 4 10^{-4} mm^3, the same obtained for NCM. In fact, from Eq. (1), the wear volume does not depend on the local contact conditions but only on the resultant force normal to the contact plane (100 N), when sliding is almost translatory and the sliding distance (total value of 400 mm) is the same for all the contact points.

The maximum contact pressure and wear depth are located at the edge fillet (point marked in red with an arrow in Fig. 5): their variations with the travelled distance are shown in Fig. 5. The contact pressure decreases rapidly during the running-in, whilst the wear depth increases non-linearly, both with trends similar to those ones at the pin axis for the NCM.

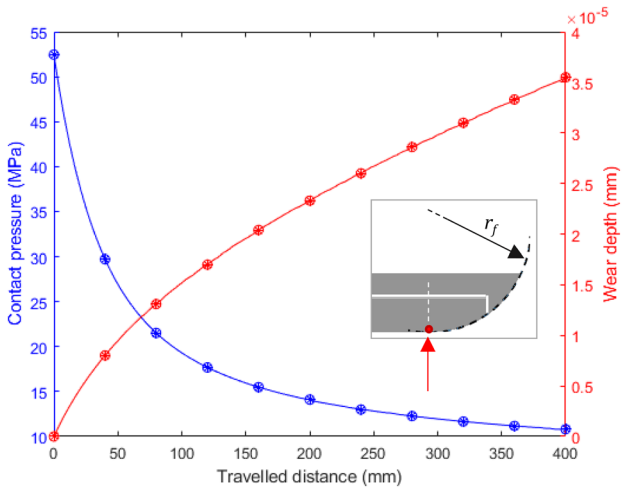

Fig. 5 Variation of the contact pressure and the wear depth at the fillet edge (point marked in red), with the travelled distance (Color figure online)

3.2.2 Effect of Friction on Wear Evolution

According to the NCM results, the effect of friction on contact/wear parameters is almost negligible: curves obtained for the frictionless and frictional cases are almost overlapped, as shown in Fig. 4 for the extreme cases $f=0$ and $f=0.4$. With respect to NCM, different considerations need to be made on the computational costs (Fig. 6). The introduction of the sliding friction causes an almost doubling of the simulation time, but this is not affected by the friction values. This might be due to the fact that the computational costs of conformal contacts mainly rely on the high number of elements in contact more than on the coefficient of friction value. Moreover, the analysis convergence of cases with $f>0.2$ required to activate Newton–Raphson unsymmetric option in non-linear control analysis which allows to reduce simulations times (Fig. 6). This option must be used with caution since, according to Ansys documentation, it can cause loss of accuracy. However, for the considered case study, it does not affect the accuracy of the results which are almost equal to the frictionless ones.

3.2.3 IK vs EK Procedures

Results obtained for IK and EK are almost identical, confirming results from NCM (Fig. 4). However, in this case, there is not a significant advantage from a computational

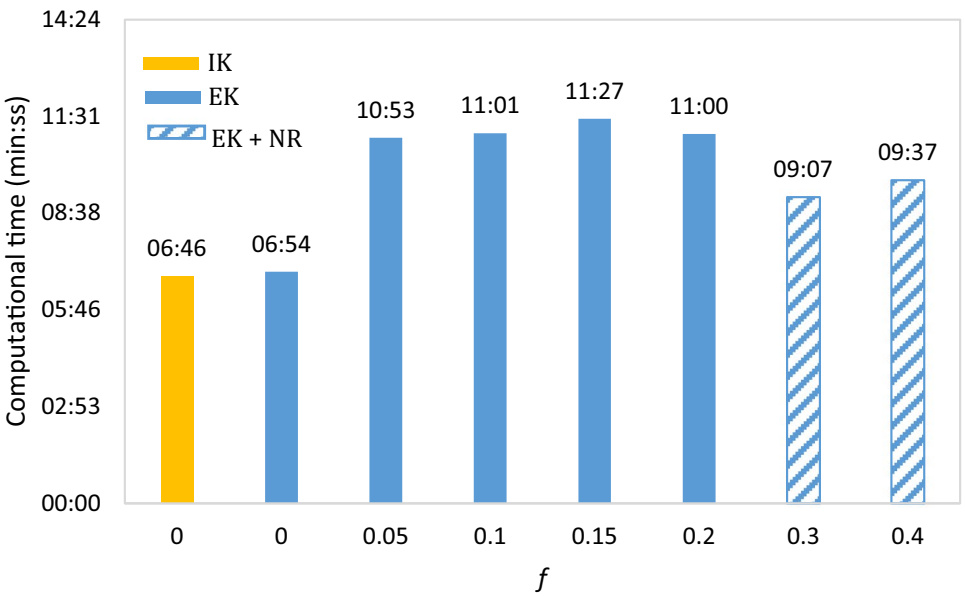

Fig. 6 Computational costs of CM simulations in function of the *f* value. Legend: NR = Newton–Raphson unsymmetric option

point of view: simulations required similar times, only a bit slower in case of IK (Fig. 6). This can be attributed to the high number of elements in contact.

3.2.4 Accelerated Simulations

In order to demonstrate that results discussed above ($N_a = 1$) remain valid even for higher wear, a total sliding distance of 20 m was also simulated, using an accelerated factor $N_a = 50$. Assuming that, wear depth at pin axis results of about 1.3 μm, i.e. very similar to the maximum wear depth for NCM. All considerations made above for the case with $N_a = 1$ remain valid for the accelerated case. In particular, frictionless and frictional ($f = 0.4$) contact simulations produced almost equal results. A graphical description of these results is not reported for brevity.

4 Conclusion

Results obtained for the non-conformal and conformal models of pin-on-plate tests were in good agreement and pointed out that the effect of the friction coefficient on contact/wear parameters is absolutely negligible, with percentage differences on pressure/wear depth values lower than 0.05% between the frictionless and the frictional contact type. Additionally, both non-conformal and conformal models confirmed the validity and usefulness of implicit kinematics simulation for the frictionless contact type, especially in case of non-conformal contact.

Considering the negligible effect of friction on wear predictions, this study suggests combining IK and frictionless contact types for wear simulations of both non-conformal and conformal pairs in frictional contact with constant sliding velocity.

Author Contributions All authors contributed to the study conception and design. FE analysis, results collection and data plotting, and manuscript writing were performed by LM. Both the authors read and approved its final version.

Funding Open access funding provided by Università di Pisa within the CRUI-CARE Agreement. The authors declare that no funds, grants, or other support were received during the preparation of this manuscript.

Declarations

Competing interest The authors have no relevant financial or non-financial interests to disclose.

References

1. Park, D., Kolivand, M., Kahraman, A.: Prediction of surface wear of hypoid gears using a semi-analytical contact model. Mech. Mach. Theory. **52**, 180–194 (2012). https://doi.org/10.1016/j.mechmachtheory.2012.01.019
2. Huang, D., Wang, Z., Kubo, A.: Hypoid gear integrated wear model and experimental verification design and test. Int. J. Mech. Sci. **166**, 105228 (2020). https://doi.org/10.1016/j.ijmecsci.2019.105228
3. Yan, Y.: Simulation on coupling effects between surface wear and fatigue in spur gear. Eng. Fail. Anal. **134**, 106055 (2022)
4. Butini, E., Marini, L., Meli, E., Rindi, A., Valigi, M., Logozzo, S.: Development and validation of wear models by using innovative three-dimensional laser scanners. Adv. Mech. Eng. **11**(8), 1687814019870402 (2019)
5. Hussin, M.S., Fernandez, J., Ramezani, M., Kumar, P., Kelly, P.A.: Analytical and computational sliding wear prediction in a novel knee implant: a case study. Comput. Methods Biomech. Biomed. Engin. **23**, 143–154 (2020). https://doi.org/10.1080/10255842.2019.1709118
6. Liu, F., He, Y., Gao, Z., Jiao, D.: Enhanced computational modelling of UHMWPE wear in total hip joint replacements: the role of frictional work and contact pressure. Wear **482–483**, 203985 (2021). https://doi.org/10.1016/j.wear.2021.203985
7. Mattei, L., Di Puccio, F., Joyce, T.J., Ciulli, E.: Numerical and experimental investigations for the evaluation of the wear coefficient of reverse total shoulder prostheses. J. Mech. Behav. Biomed. Mater. **55**, 53–66 (2016). https://doi.org/10.1016/j.jmbbm.2015.10.007
8. Mattei, L., Di Puccio, F.: Wear Simulation of metal-on-metal hip replacements with frictional contact. J. Tribol. **135**, 021402 (2013). https://doi.org/10.1115/1.4023207
9. Mary, C., Fouvry, S.: Numerical prediction of fretting contact durability using energy wear approach: optimisation of finite-element model. Wear **263**, 444–450 (2007). https://doi.org/10.1016/j.wear.2007.01.116
10. McColl, I.R., Ding, J., Leen, S.B.: Finite element simulation and experimental validation of fretting wear. Wear **256**, 1114–1127 (2004). https://doi.org/10.1016/j.wear.2003.07.001
11. Bose, K.K., Penchaliah, R.: Finite element method based sliding wear prediction of steel-on-steel contacts using extrapolation techniques. Proc. Inst. Mech. Eng, Part J: J. Eng. Tribol. **233**(10), 1446–146318 (2019)
12. Bastola, A., Stewart, D., Dini, D.: Three-dimensional finite element simulation and experimental validation of sliding wear. Wear **504–505**, 204402 (2022). https://doi.org/10.1016/j.wear.2022.204402
13. Shankar, S., Nithyaprakash, R., Santhosh, B.R., Uddin, M.S., Pramanik, A.: Finite element submodeling technique to analyze the contact pressure and wear of hard bearing couples in hip prosthesis. Comput. Methods Biomech. Biomed. Engin. **23**, 422–431 (2020). https://doi.org/10.1080/10255842.2020.1734794

14. Curreli, C., Di Puccio, F., Mattei, L.: Application of the finite element submodeling technique in a single point contact and wear problem. Int. J. Numer. Methods. Eng. **116**, 708–722 (2018). https://doi.org/10.1002/nme.5940
15. Di Puccio, F., Mattei, L.: A novel approach to the estimation and application of the wear coefficient of metal-on-metal hip implants. Tribol. Int. **83**, 69–76 (2015). https://doi.org/10.1016/j.triboint.2014.10.023
16. Kang, L., Galvin, A.L., Fisher, J., Jin, Z.: Enhanced computational prediction of polyethylene wear in hip joints by incorporating cross-shear and contact pressure in additional to load and sliding distance: effect of head diameter. J. Biomech. **42**, 912–918 (2009). https://doi.org/10.1016/j.jbiomech.2009.01.005
17. Mattei, L., Di Puccio, F., Ciulli, E., Pauschitz, A.: Experimental investigation on wear map evolution of ceramic-on-UHMWPE hip prosthesis. Tribol. Int. **143**, 106068 (2020). https://doi.org/10.1016/j.triboint.2019.106068
18. Mattei, L., Di Puccio, F.: Influence of the wear partition factor on wear evolution modelling of sliding surfaces. Int. J. Mech. Sci. **99**, 72–88 (2015). https://doi.org/10.1016/j.ijmecsci.2015.03.022
19. Wang, L., Isaac, G., Wilcox, R., Jones, A., Thompson, J.: Finite element analysis of polyethylene wear in total hip replacement: a literature review. Proc. Inst. Mech. Eng. **233**, 1067–1088 (2019). https://doi.org/10.1177/0954411919872630
20. Bartel, D.L., Burstein, A.H., Toda, M.D., Edwards, D.L.: The effect of conformity and plastic thickness on contact stresses in metal-backed plastic implants. J. Biomech. Eng. **107**, 193–199 (1985). https://doi.org/10.1115/1.3138543
21. Man, K.W., Aliabadi, M.H., Rooke, D.P.: BEM frictional contact analysis: Modelling considerations. Eng. Anal. Bound. Elem. **11**, 77–85 (1993). https://doi.org/10.1016/0955-7997(93)90081-U
22. Lengiewicz, J.: Efficient model of evolution of wear in quasi-steady-state sliding contacts. Wear **303**(1–2), 611–621 (2013)